Available online at www.sciencedirect.com
SCIENCE DIRECT
Tectonophysics 421 (2006) 251–267
TECTONOPHYSICS
www.elsevier.com/locate/tecto

The effects of a lateral variation in lithospheric strength on foredeep evolution: Implications for the East Carpathian foredeep

K.A. Leever [a,b,*], G. Bertotti [a], R. Zoetemeijer [a], L. Matenco [b], S.A.P.L. Cloetingh [a]

[a] *Department of Tectonics, Faculty of Earth and Life Sciences, Vrije Universiteit Amsterdam De Boelelaan, 1085 1081 HV Amsterdam, The Netherlands*
[b] *Netherlands Research Centre for Integrated Solid Earth Science (ISES), Vrije Universiteit Amsterdam De Boelelaan, 1085 1081 HV Amsterdam, The Netherlands*

Received 30 November 2005; received in revised form 19 April 2006; accepted 28 April 2006
Available online 21 June 2006

Abstract

Lateral variations in lithospheric strength have been adopted often in flexural modeling (both 2D and 3D) to better fit the observed basement deflections, typically supported by gravity data. This approach provides essentially a "snap-shot" of the role of lithosphere strength in determining the present day geometry.

In contrast, we investigate and quantify the effects of a lateral change in lithospheric strength on the evolution of the foredeep in front of an advancing orogen. Transitions in lithospheric strength are common in the foreland of orogens and show large variations in the width of the transition zone and the strength difference. Former passive margins, for instance, will display strength changes distributed over several tens to hundreds of kilometers. Other transitions may originate from juxtaposition or accretion of pieces of lithosphere with different properties and may be characterized by a much smaller width than former passive margins.

In our modeling, a constant load, representing an advancing orogenic belt, is displaced towards and across a transition from a weak to a strong plate in a 2D elastic thin plate model. The effect of different transition widths and strength contrasts on foredeep geometry and bending stress is investigated. Interference of flexural wavelengths across the transition affects foredeep geometry by causing rapid basin widening, oscillation of the bulge and volume increase. The bending stresses are found to concentrate and amplify around the strength transition. Large transition gradients, i.e. large strength contrast or small transition width, cause the highest rates of change.

Basin widening caused by the orogenic load advancing towards the transition between the East European Craton and the Moesian Platform, appears to control the Sarmatian transgression over the East Carpathian foreland in Romania.

Keywords: Flexure; Foreland basin; Lithosphere strength; East Carpathians

1. Introduction

The notion that the strength of the (continental) lithosphere is hardly uniform (Fig. 1a), both in time and in space, has been recognized in many previous studies on the forelands of orogens such as the Pyrenees (Aquitaine Basin (Desegaulx et al., 1991)), the Rocky Mountains in Alberta, Canada (Wu, 1991), Appalachians (Stewart and Watts, 1997), West and East Carpathians (Matenco et al., 1997; Zoetemeijer et al., 1999) and the Caledonian Baltic Basin (Lazauskiene et al., 2002)). The non-constant flexural rigidity of the lithosphere (expressed by

* Corresponding author. Tel.: +31 20 598 72 78; fax. +31 20 598 9943.
E-mail address: karen.leever@falw.vu.nl (K.A. Leever).

0040-1951/$ - see front matter © 2006 Elsevier B.V. All rights reserved.
doi:10.1016/j.tecto.2006.04.020

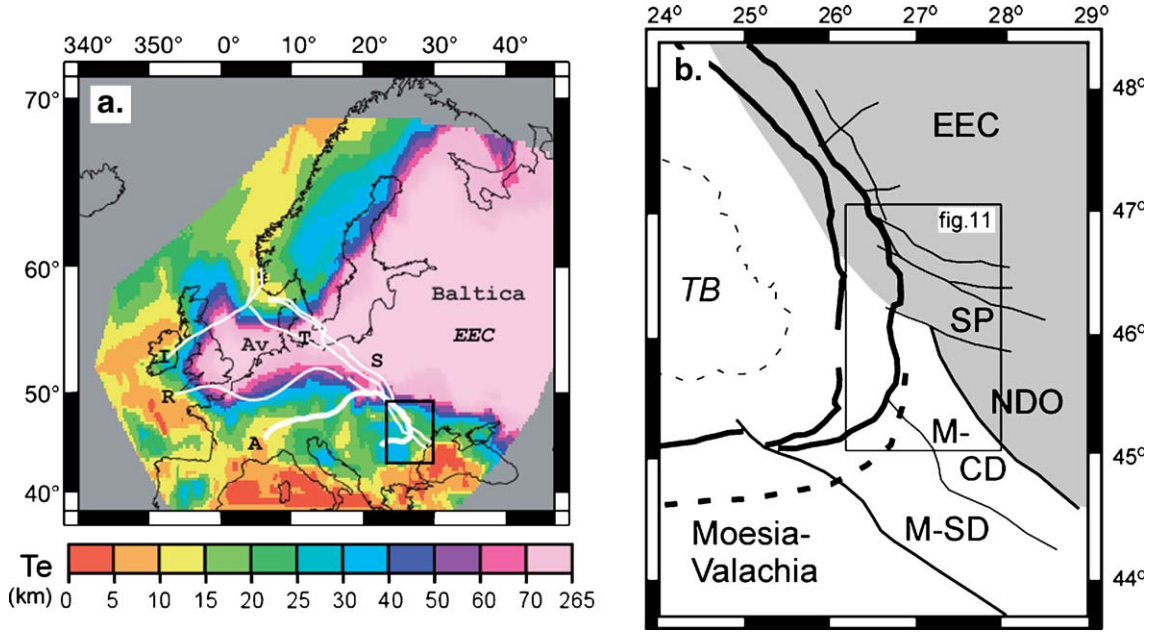

Fig. 1. (a) Elastic thickness map of the European lithosphere showing large strength variations, adapted from Pérez-Gussinyé and Watts (2005). Te values are obtained from Bouguer coherence method. Note the large strength change in the East Carpathian foreland. Study area is indicated by black rectangle. White lines indicate sutures: I, Iapetus; T, Thor; R, Rheic; S, Sorgenfrei-Tornquist and Tornquist-Teisseyre zones. Thick white line is Alpine deformation front. EEC is East European Craton; Av, Avalonia. (b) Foreland of the East Carpathians. EEC, East European Craton; SP, Scythian Platform; NDO, North Dobrogean Orogen; M–ND, Moesian Platform–North Dobrogea; M–CD, Moesian Platform–Central Dobrogea. TF, Trotus Fault; PCF, Peceneaga–Camena Fault.

differences in effective elastic thickness, Te) has been widely used in flexural modeling to explain the observed present-day basement deflection caused by (orogenic) loading of the lithosphere (Bodine et al., 1981; Royden and Karner, 1984; Matenco et al., 1997; Zoetemeijer et al., 1999). This approach provides essentially a "snapshot" of the role of lithosphere strength in determining the present day geometry.

However, in a peripheral foredeep setting (pro-foredeep sensu Willett et al., 1993; Johnson and Beaumont, 1995), the foredeep is situated on the subducting plate and hence is progressively displaced towards the orogen, causing a forelandward migration of the foredeep depozones (DeCelles and Giles, 1996). A spatial variation of lithosphere strength will thus influence the temporal evolution of a foreland basin, as has been demonstrated by Stockmal et al. (1986) and Waschbusch and Royden (1992).

Spatial transitions in strength can be gradual or abrupt. Gradual changes are typically associated with a pre-orogenic history of rifted margin formation, whereas juxtaposition of different tectonic units may lead to more abrupt transitions.

The variation in lithosphere properties caused by a former rifting stage will generally be perpendicular or at a high angle to the new convergent margin. The width of the thinned lithosphere in a passive margin is highly variable with widths between 50 and 600 km, but it may be as small as 10–20 km (Davison, 1997). The presence of a former passive margin in the foreland of an evolving orogen will influence foredeep evolution in several ways. Firstly, rifting causes thinning and therefore (initial) weakening of the continental lithosphere of the plate that is later to be subducted. It must be noted that the time elapsed between rifting and the contractional stage determines the thermal state of the passive margin and hence the relative strength and buoyancy of the lithosphere (Stockmal et al., 1986). A young margin is characterized by a hot thin lithosphere that is relatively weak and buoyant, while the lithosphere of the old margin has cooled down and as a consequence become thicker, stronger, and less buoyant (e.g. Bertotti et al., 1997; Van Wijk, 2002). Because of the large variability in thermal lithospheric structures, the duration of these changes and, therefore, the mechanical state of specific lithospheric segments are matters of discussion (Burov and Diament, 1995; Bertotti et al., 1997). A second effect (Desegaulx et al., 1991) related to rifting and contributing to the lithosphere deflection is the larger initial water depth on the passive margin: the isostatic

adjustment to rifting causes subsidence of the plate and a corresponding larger initial accommodation space for sediments. Both effects will result in a deeper foredeep with respect to unstretched lithosphere. Finally, the normal faults in the passive margin may be reactivated by the flexure of the lithosphere during later orogenic loading, potentially changing the shape of the deflection (Zoetemeijer, 2000).

Abrupt transitions in lithosphere strength at various angles to the convergent margin can be expected as a result of inherited structure of the lithosphere (Stewart and Watts, 1997). Large transform structures can juxtapose lithosphere plates with different ages and properties. An example of such an inherited structure is the Tornquist–Teysseire zone (TTZ) which represents the southwestern margin of Baltica and the East European Craton (EEC). It is a dextral shear zone that accommodated as much as 1000 km of displacement in Paleozoic times (Pharaoh, 1999). As a consequence, it is a zone where the undisturbed Proterozoic lithosphere of Baltica is juxtaposed to more recently accreted (but most likely Baltica derived) terranes such as the Malopolska and Lysogory terranes in Poland (accretion between Cambrian–Carboniferous) and the Moesian Platform in Romania. It is inferred to continue below the East Carpathian deformation front. During their Miocene final emplacement, the East Carpathians thus encountered a laterally strongly varying foreland lithosphere (Fig. 1b).

In this paper we will quantify the effect of a spatial lithospheric strength transition on foredeep evolution, expressed by changes in basin geometry and bending stress. We investigate how spatial differences in lithosphere flexural strength can explain the observed temporal changes in foredeep geometry. We used a 2D elastic finite difference code to model the effect of different parameters, comprising the width and the contrast of the transition. The modeling results are then applied to the East Carpathian foredeep, which during its evolution experienced pronounced changes in its shape (Tărăpoancă, 2004). Of the main processes influencing basin evolution (Johnson and Beaumont, 1995) we will hence discuss only the flexural isostatic response, neglecting the effects of the rates of convergence, surface transport and sedimentation, and eustasy, the significance of which has been proven by other authors (Flemings and Jordan, 1989; Johnson and Beaumont, 1995, Garcia-Castellanos, 2002; Clevis et al., 2004).

We find that across the transition, the shape of the foredeep basin does not change gradually from a geometry characteristic for the weak plate to a geometry characteristic for the strong plate, but rather in a stepwise manner or initially even in the opposite sense than would be expected. The rates and magnitudes of the changes are greatest for the largest transition gradient: small transition width and large strength contrast. A consistent correlation between changes in basin width, volume and stress is observed. Throughout this paper, 'strength' is treated in terms of flexural rigidity of the plate expressed by its effective elastic thickness Te, which represents the plate stiffness rather than its resistance to failure (Ranalli, 1995).

2. Modelling strategy and method

In our modeling we aim to quantify the effect of a change in plate strength, expressed in its effective elastic thickness (Te), on the evolution of foredeep geometry and stress distribution and magnitude as functions of the flexural response to an advancing orogen. To this end, we quantify the influence of several parameters: the width of the strength transition, the strength contrast between the plates, and the size of the load, the results of which are presented in Section 3.1–3 respectively.

2.1. Flexure and elastic rheology

2.1.1. Wavelengths and amplitudes

Previous studies have demonstrated (Watts et al., 1980; Ranalli, 1995) that the behaviour of an elastic thin plate is a good first order approximation of the behaviour of the lithosphere when subjected to vertical or horizontal loads, which cause flexure and buckling respectively. For derivation of the 4th order differential equation of flexure, see chapter 3.16 in Turcotte and Schubert (2002) or Bodine and Watts (1979).

$$\mathrm{d}^2/\mathrm{d}x^2[D(x)\mathrm{d}^2w/\mathrm{d}x^2] + N\mathrm{d}^2w/\mathrm{d}x^2 + \rho_m g w(x) = q_a(x) \quad (1)$$

Fig. 2 shows the basin margin and bulge positions resulting from analytically solving the flexure equation for both an air filled and a sediment filled basin. The amplitude of the deflection, i.e. w_0 and the corresponding bulge elevation, are dependent on both the size of the load V_0 and the flexural rigidity D.

In general, the larger Te and the smaller the density contrast between mantle and basin infill, the wider the basin and the shallower the deflection will be. In our results (Section 4) we show how the basin wavelength adapts to the encountered strength difference.

2.1.2. Bending stresses

The 2D elastic thin plate model we apply is based on the assumptions that (1) the properties in the third dimension (perpendicular to the section) are constant

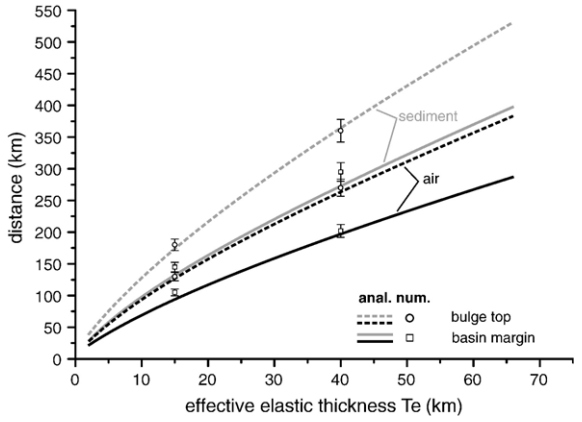

Fig. 2. Flexural wavelength as a function of Te for basin fill of air (0 kg/m^3) and sediment (2400 kg/m^3). Lines: analytical solutions for position of the basin margin [$w(x)=0$ at $x=0.75\ \pi\alpha$] and top of bulge [$w'(x)=0$ at $x=\pi\alpha$]. Open symbols: numerical solutions (with 5% error bars). $w=w_0\ e^{-x/\alpha}\ (\cos x/\alpha+\sin x/\alpha)$, where w_0 is the deflection at $x=0$: $w_0=[V_0\ \alpha^3]/[8D]$ and α is the flexural parameter: $\alpha=[4D/\rho_m\ g]^{1/4}$.

over a large distance and (2) that the plate consists of uniform material, with a linear elastic rheology. The bending stresses (or fiber stresses, σ_{xx} or σ_x) we calculated and discuss in the subsequent sections, are longitudinal stresses at the top of the plate, in the x-direction of the reference frame. This is one component of the stress tensor only and can thus be represented by a scalar number (MPa).

Due to loading, the plate deforms by bending (Fig. 3). A surface of zero stress (neutral surface) is located in the middle of the plate, its location defined by the uniform properties of the plate from top to base. Above this surface, stresses are tensional for a convex shape and compressional in the concave case. The magnitude of these stresses is a function of the curvature of the plate: the larger the curvature, the larger the longitudinal strains and the larger the resulting stresses; in the following relationship:

$$\sigma_x = E\varepsilon_x = E\kappa y = \tfrac{1}{2}E\kappa \mathrm{Te} \qquad (2)$$

where σ_x is longitudinal stress (in x direction), E is Young's Modulus, ε_x is longitudinal strain (in x direction), κ is curvature and y is the vertical distance to the neutral surface. For derivation see Gere (2001). In our case, y is equal to ½ Te, since the neutral surface is located in the middle of the plate. As seen in the previous section, the curvature (and thus the bending stress) is a function of flexural rigidity D and load size V_0: relatively large bending stresses will result from a weak plate or a large load.

As pointed out by Watts et al. (1980) from results of rock mechanics studies, the magnitudes of the stresses predicted by a pure elastic rheology are too large to be realistic: in nature failure will occur before values in the order of 1 GPa are reached.

2.2. Modelling

2.2.1. Model characteristics

The code we used is COBRA (see Zoetemeijer et al., 1999, for details), which offers a 2D solution of the 4th order flexural differential equation. It allows for different load sizes, variation in elastic thickness, incorporation of a passive margin and corresponding initial water depth.

We adopted an elastic thin plate model because we want to focus on the effects of lateral strength changes. By doing so, we will not take into account the effects of other processes such as mass redistribution at the surface and eustasy (Flemings and Jordan, 1989; Johnson and Beaumont, 1995). We furthermore assume the lithosphere strength to be constant with time.

2.2.2. Model stability

Tests were run to prove the model stability. Model stability was proven for a finite difference step size of 10 km: a total of 200 nodes thus results in model dimension of 2000 km, which is sufficiently wide to avoid edge effects as the load keeps a minimum distance to the model edge of 800 km, more than twice the distance between bulge top and load for a plate with a Te of 40 km (Fig. 2). Fig. 2 shows the basin margin and bulge top positions resulting from analytically solving the flexure equation, both for an unfilled basin and for a sediment filled basin. The smaller density contrast in the sediment filled basin leads to a wider basin or larger wavelength. As such, an unfilled basin on a plate with a Te of 28 km will result in the same basin width (bulge position at 200 km) as a sediment filled basin on a plate with a Te of 18 km. In the figure we also show some numerical test results (open symbols) with 5% error bars. They fit well to the analytical solution in the air-filled

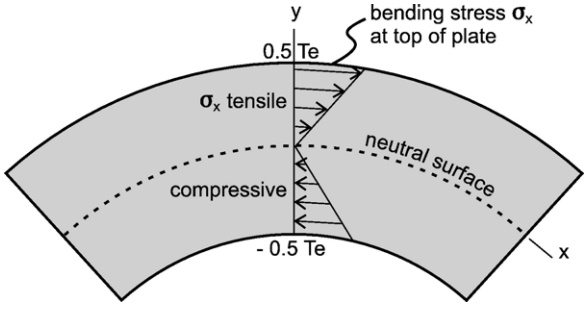

Fig. 3. Bending stresses inside a flexed plate.

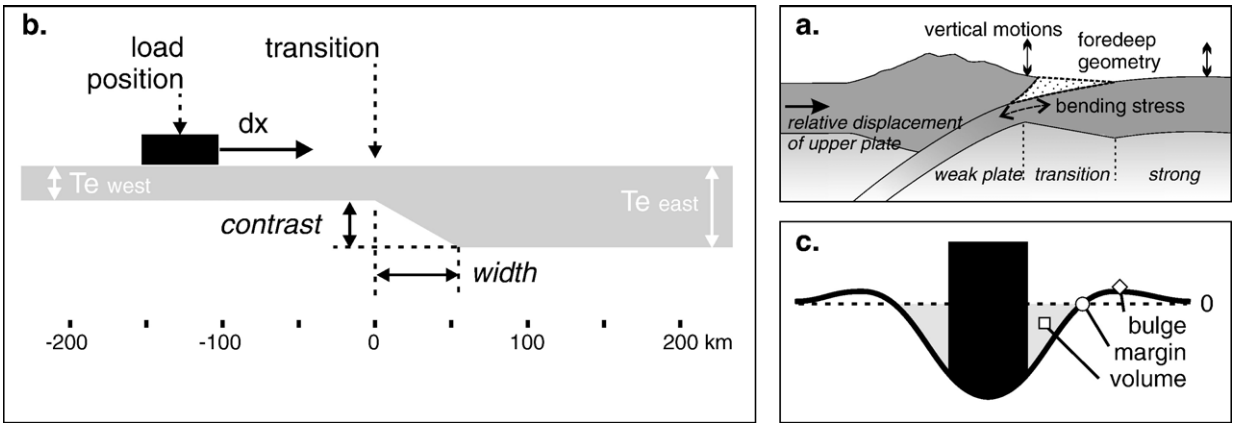

Fig. 4. (a) Cartoon showing lithospheric strength transition and the parameters quantified in this paper (b) Model setup including tested parameters (in italics), and (c) variables used to quantify basin geometry. For explanation see text and Table 1.

case. For a sediment filled basin, the numerical and analytical results do not agree well, mainly on the position of the basin margin. This is due to the fact that the analytical method assumes a constant density contrast along the whole length of the model, while the numerical approach is able to distinguish laterally between the sediment-filled basin and the other portions of the model that are overlain by air. The numerical solution should be preferred over the analytical one in this case.

2.2.3. Model setup

The general model setup for all runs is shown in Fig. 4 and Table 1. The location of the strength transition zone is defined by the position of its left-hand (westward) termination. The orogenic load is represented by a block of 50 km wide and 2 km high. We chose to apply a constant load because we want to concentrate on the effect of the strength transition only. Its position is defined by the position of its center (initially at −200 km). It is displaced towards the east by steps of 10 km, small enough to capture the changes induced by the migrating load. For the parameter values tested in the different model runs see Table 1.

3. Modeling results

A first impression of the progressive foredeep evolution across a strength transition is given in Fig. 5a. It shows the foredeep shape across the 20-km wide strength transition at 20 load steps between the initial load position at $x=-200$ km and the final position at $x=200$ km. The non-linear character of the changes in basin geometry across the strength transition is qualitatively evident from this figure. The basin is rapidly shallowing and widening; the bulge elevation oscillates. The bending stresses are derived from the plate deflection: we calculated the maximum tensile stresses and their positions on the eastern flank of the basin. Note that the location of maximum stress (i.e. maximum curvature) is not associated with the forebulge, but rather occurs at a deeper level on the basin flank. This is illustrated in Fig. 5b for a plate of constant strength (Te=15 km). Exaggeration of the vertical scale in Fig. 5a changes the apparent position of maximum curvature.

These changes are discussed in more detail in the following sections. We present our modeling results, showing the effect of the transition width (3.1) and contrast (3.2) on basin geometry and bending stress. The general pattern is similar (cf. Fig. 5) for all cases: the bottomline is that the system has to change between the

Table 1
(a) Model setup and (b) tested parameters

a) Setup

Model domain (km):	−1000 to 1000	Densities (kg/m^3):	
Transition position (x):	0	Basin infill	2400
Load displacement:		Load	2800
Start (x):	−200	Crust	2800
Stop (x):	200	Mantle	3300
Displacement increment:	10 km	Young's modulus:	70 GPa
		Poisson's ratio:	0.25

b) Tested parameters

Model runs:	Width	Contrast (Te west; Te east)	
4.1: Transition width	0, 20, 50, **100**, 200	**15**	40
4.2: Contrast	20	10, 15, 18, 21	40

Parameters for the Carpathians reference model are shown in bold face.

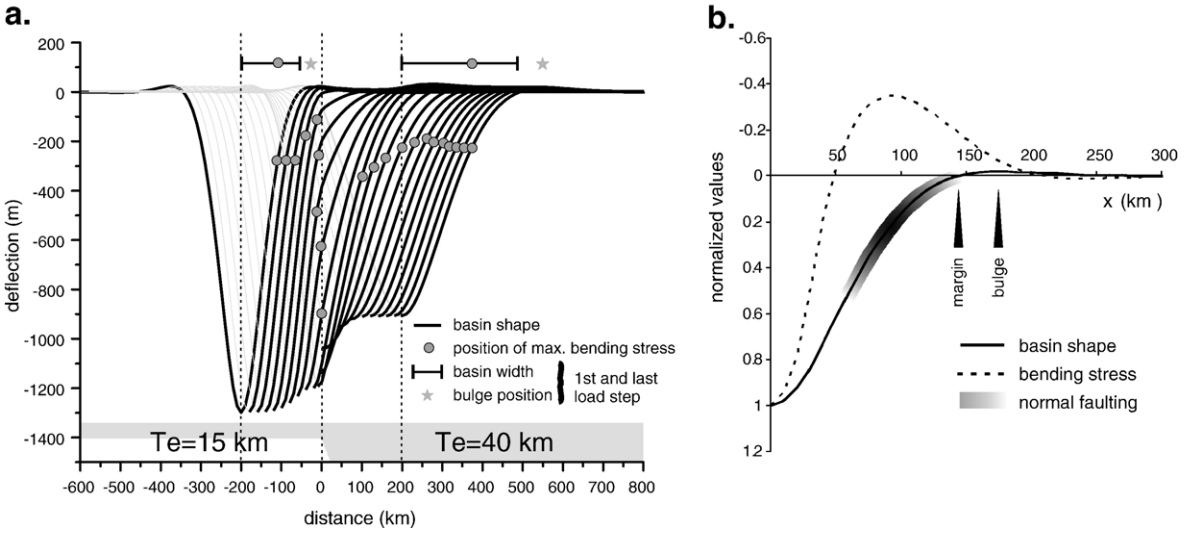

Fig. 5. (a) Changing basin shape as an effect of progressive loading across a 20-km wide transition from Te=15 km to Te=40 km. See text for explanation. (b) Normalized deflection and bending stress in a plate of Te=15 km showing the position of (max.) bending stress with respect to the basin margin/bulge.

equilibria on each side of the transition. However, the rates and magnitudes are different depending on the transition gradient. To demonstrate this, we quantify the changes in basin geometry (Fig. 4c) by extracting 1) the position of the basin margin, 2) position and elevation of the top of the forebulge, and 3) the cross sectional area (volume of the basin). Changes in the stress pattern are monitored by calculating the location and magnitude of the maximum bending stresses at the top of the plate. The results are mostly shown as a function of the position of the load with respect to the strength transition (Figs. 6–10). Load steps at which major changes occur are indicated by numbered arrows.

3.1. Width of the transition

We ran a series of models testing the influence of the width of a transition in effective elastic thickness (Te) on foredeep geometry and stress distribution. The Te of the western and eastern part of the plate is set at 15 and 40 km respectively (Fig. 4b). These values are based on those inferred for the Moesian Platform and East European Craton (Tărăpoancă, 2004). We tested five different transition widths (Table 1) of 0, 20, 50, 100 and 200 km. A constant load (2 km thick, 50 km wide) was displaced by 10-km increments towards the east. For each load step the plate deflection and bending stress were calculated.

3.1.1. Basin geometry

Fig. 6 shows how the basin geometry adapts, as the load moves eastward towards and across the strength transition, from the equilibrium in the western plate (Te=15 km) to the equilibrium in the eastern plate (Te=40 km). In a homogeneous plate, the migration of the basin margin (and bulge) would occur at a constant rate equal to the load migration rate. Across the strength transition (Fig. 6a) the rate increases: the basin is widening (Fig. 6b) due to the larger flexural wavelength characteristic for the stronger plate (150 km for Te15, 290 km for Te40, Fig. 2).

Basin widening initiates when the load is at a distance of 180 km from the transition (loadstep 1). It occurs at a constant rate of ca. 1.5 times the load migration rate for the 200-km wide transition. The other cases show a stepwise increase: two periods of widening are separated by a period of constant or even decreasing basin width (Fig. 6b). The highest rates of change are recorded by the narrow transitions: when the load is displaced by 30 km from $x=-150$ to $x=-120$, the basin margin migrates by 110 km (for 0-km wide transition, Fig. 6a), resulting in a basin widening of 80 km (Fig. 6b). Toward $x=0$ the migration rates for the 0-, 20- and 50-km wide transitions are approximately equal at ca 0.8 times the load migration rate (load steps 3–4). For this period, the basin margin thus migrates slower than the load and the basin is narrowing. The basin width is constant during these load steps for the 100-km wide transition zone. A second increase (with rates up to 1.8, around load step 5) follows until at $x>120$ km the basin width corresponding to the Te=40 wavelength is attained and margin migration is again equal to the load migration (load step 7).

Non-linear evolution is also shown by variations in the bulge elevation (Fig. 6c). Instead of a gradual transition between the values characteristic for an elastic thickness of 15 and 40 km, the bulge elevation first drops well

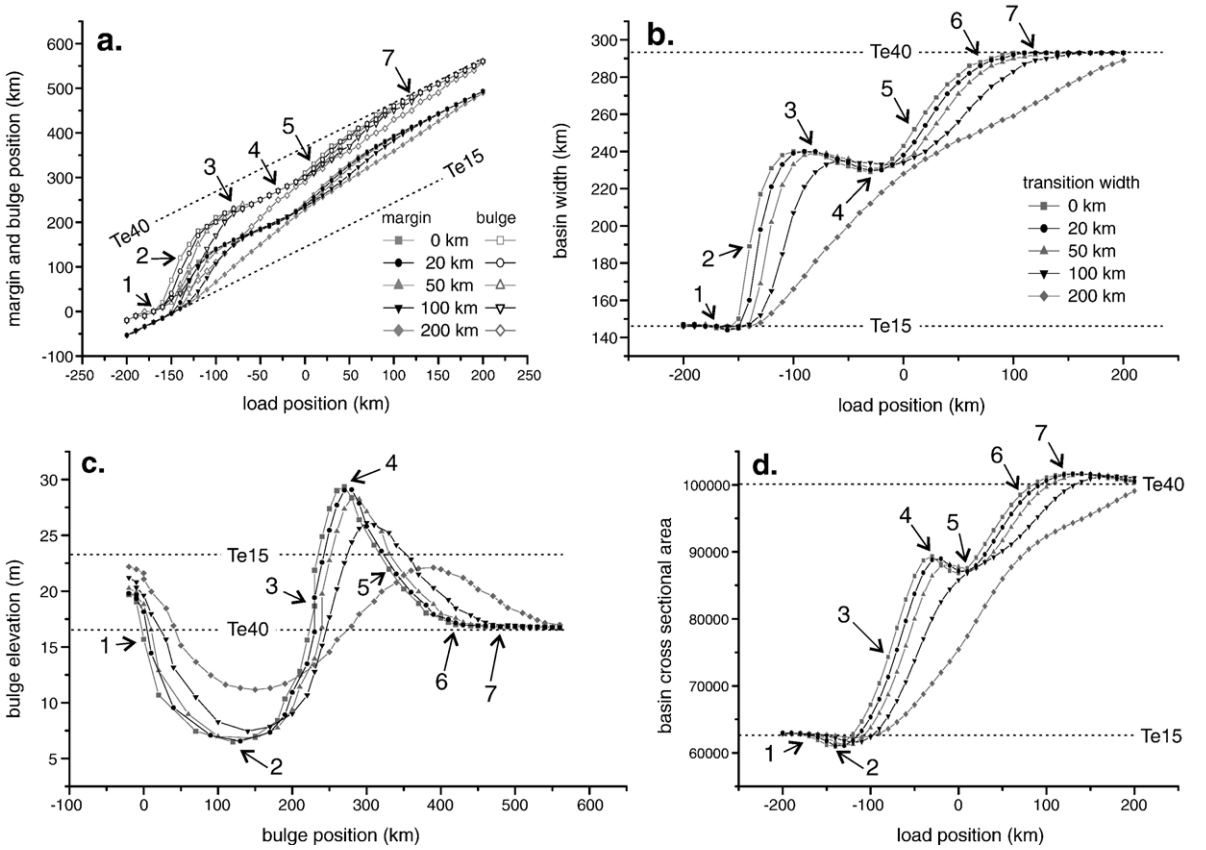

Fig. 6. Changing basin geometry for different transition widths as a function of load position. Here and in Figs. 7–9: dashed lines indicate equilibrium values for the western and eastern plate strengths respectively. Selected, correlating, load steps at which specific events take place during progressive basin evolution are marked by numbered arrows and discussed in the text. Refer to Fig. 5 for the general expression of the changes quantified in this figure and Figs. 7–9. (a) Migration of margin and bulge; (b) basin width (distance from center of load to basin margin). Note rapid basin widening in two steps separated by period of constant or even decreasing basin width for the narrow transitions, and widening at constant rate for the 200-km wide transition; (c) elevation of the bulge as a function of its position. Note oscillation instead of steady decrease to Te40 equilibrium; and (d) cross section area or volume showing similar pattern as basin width.

below the Te40 value (load step 2). It subsequently increases to a maximum value (load step 4) larger than the characteristic Te15 bulge elevation before it finally settles at the new equilibrium value. Only for the 200-km wide transition the bulge elevation does not exceed its original equilibrium value.

In the basin cross sectional area (representing volume) a similar trend as in the margin and bulge positions is observable (Fig. 6d). When the load is between $x \sim -200$ and -100 km, the basin volume hovers around the Te15 value. A rapid, stepwise, increase follows until the Te40 equilibrium volume is attained. The maximum rate of volume increase occurs at load step 3.

3.1.2. Bending stress

Bending stresses at the top of the plate are calculated at each load step and for each node from the curvature of the deflected plate. In Fig. 7a shows the position of maximum stress as a function of the load position. For a plate of constant Te, and during the initial load steps of our model, the position of the maximum stress is constant with respect to the load (cf the position of the basin margin). With a transition in elastic thickness, during progressive convergence the distance between the load and the position of the maximum stress (Fig. 7a) is no longer constant. When the load has reached a distance of ~ 120 km to the transition, the migration of the maximum stress is halted. For as long as 10 load steps or 100 km of displacement, the maximum stress is fixed at the eastern edge of the Te transition. With progressive load displacement, the maximum stress does not gradually decrease from the Te15 to the Te40 values (Fig. 7b, c). Instead, it sharply increases during the period it is fixed along the strength transition. The

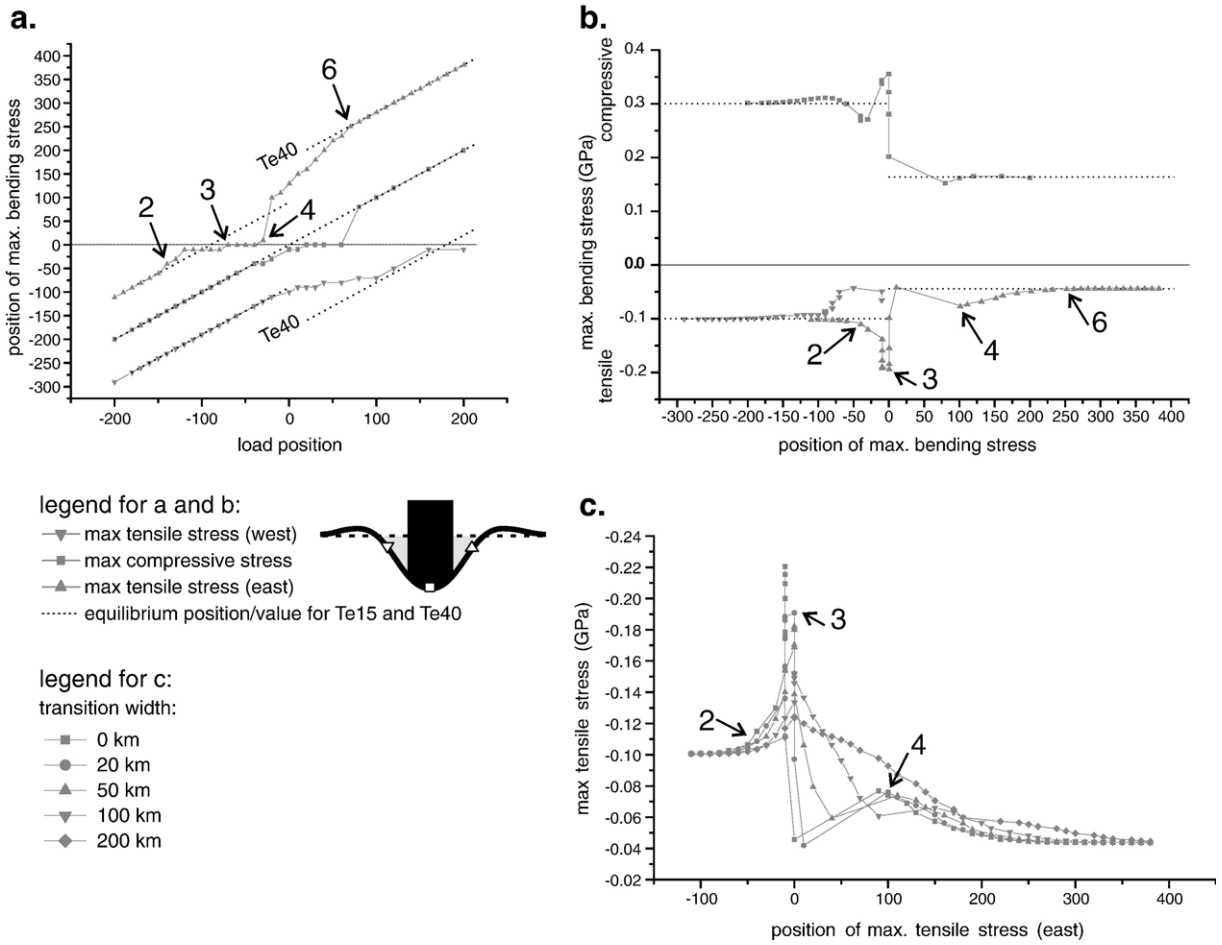

Fig. 7. (a) Position of maximum bending stresses as a function of load position for the 20-km wide transition. The maximum tensile stress on the eastern basin flank remains fixed at the strength transition while the load is displaced by 100 km. (b) Magnitude of maximum bending stresses as a function of stress position for the 20-km wide transition. (c) Magnitudes of maximum tensile stress situated on the eastern basin flank as a function of stress position for 5 different gradients. Note negative values on stress magnitude axis. (See also caption of Fig. 6).

maximum compressive stress increases from 300 to 355 MPa, the maximum tensile stress on the eastern flank even almost doubles from −100 to −190 MPa (load step 3). Only when the load reaches a distance of 30 km to the transition (load step 4) the maximum stress moves away from the transition; first rapidly, then more gradually, before reaching the Te40 equilibrium distance to the load. The corresponding decrease to the Te40 equilibrium value, which was initially rapid, is gradual from this point (Fig. 7b, c, load step 4). The highest stress value is thus recorded several load steps before the position of the maximum stress shifts away from the transition.

For the other transition widths (Fig. 7c), the pattern of stress change is similar to the 20-km wide transition discussed above: all show an increase in the maximum stress value before it decreases to the new Te40 equilibrium value. The largest maximum stress value is attained for the 0-km transition width. Even the 200-km wide transition shows a small stress increase.

3.2. Strength contrast

We tested several strength contrasts additional to the 15–40 km contrast in the previous model runs by varying the Te of the western plate (Table 1). The transition width was kept constant at 20 km. All other parameters such as size and displacement of the load are the same as in the previous experiment.

3.2.1. Basin geometry

Modifications in basin width are shown in Fig. 8a. All strength contrasts show the same basin widening trend; however, the effect is most pronounced for the

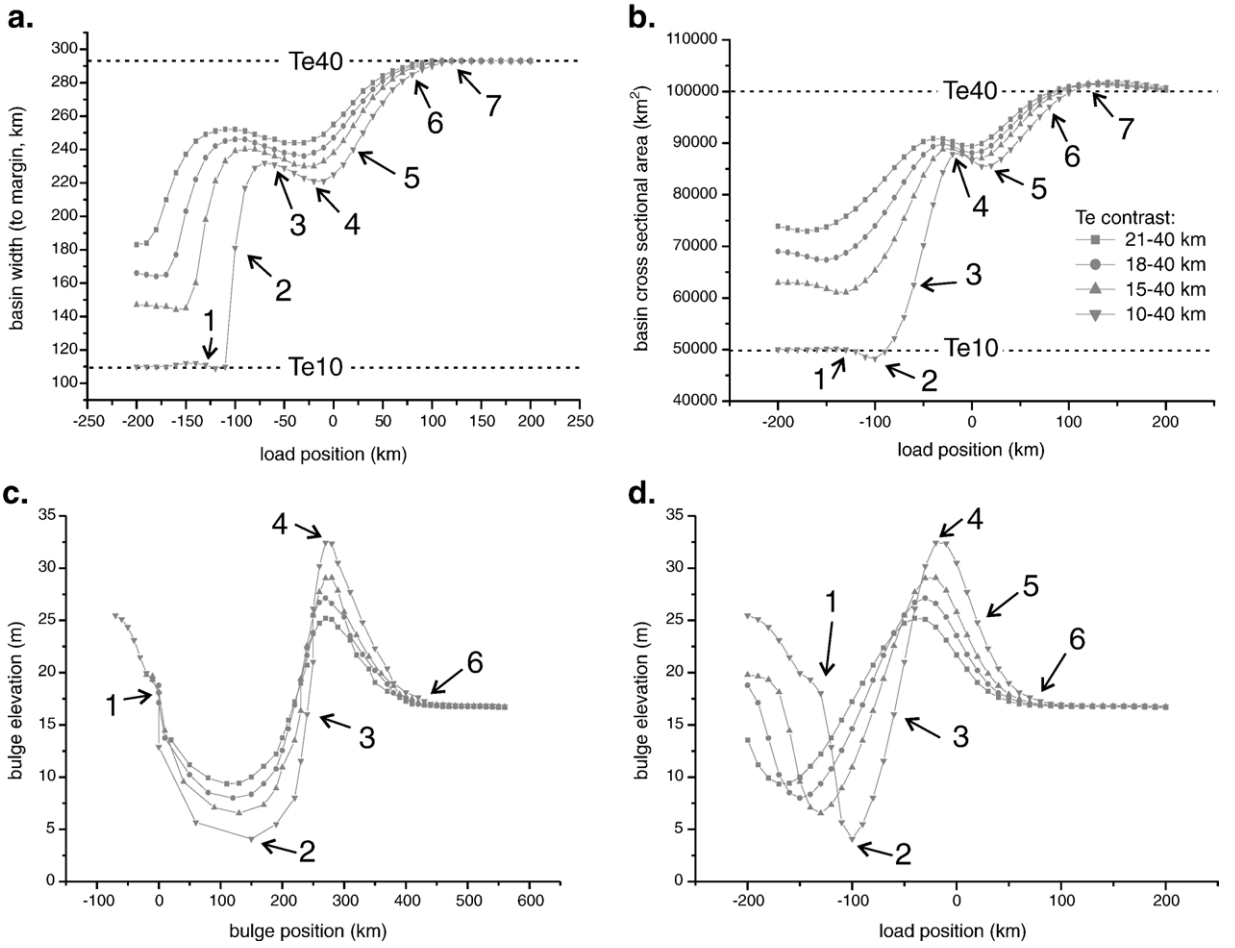

Fig. 8. Changing basin geometry for different strength contrasts as a function of load position. (a) Margin position, (b) basin cross sectional area (representing basin volume), (c) bulge elevation as function of bulge position, (d) bulge elevation as function of load position. (See also caption of Fig. 6).

large contrast (10–40 km). As for the previous model runs, the basin width is initially constant when the load is still far from the transition. This stage is followed by rapid basin widening, starting at a distance from the transition that is determined by the rigidity of the western plate, varying between ~ 110 km for the 10–40 km contrast and ~ 200 km for the 21–40 contrast.

The influence of the transition contrast on the rate of basin widening is twofold. With the rigidity constant at 40 km in the east, a small Te in the western part of the plate firstly causes a large difference in equilibrium basin width. Secondly, because of more localized deformation in this weak part, the effect of the plate transition is only felt at a very late stage. These effects add up: a relatively large difference in wavelength has to be overcome in a relatively small number of load steps. The extreme case we tested (transition from 10 to 40 km) illustrates this well: while the load migrates by merely 30 km (from $x=-110$ to $x=-80$), the basin width increases by 120 km (from 110 km to 230 km).

In Fig. 8b the basin cross sectional area is shown. The greater the strength contrast, the greater the difference between the equilibrium volumes: the Te40 volume is twice the Te10 volume. As for the basin width, the onset of volume increase occurs closer to the transition for a weak western plate, and the rate of volume increase is greatest for the 10–40 contrast. At its maximum rate (load step 3, between $x=-70$ km to $x=-40$ km) it increases by 12% per 10 km of load displacement.

As the Te transition width and position are equal for all tested contrasts, the minimum and maximum bulge top elevations occur in the same position (at $x\sim120$ km and $x\sim275$ km respectively) for each contrast (Fig. 8c). Note however that the load positions for which these maximum elevations are reached are different (Fig. 8d): in the 10–40 case, the load is at $x=-100$ km for

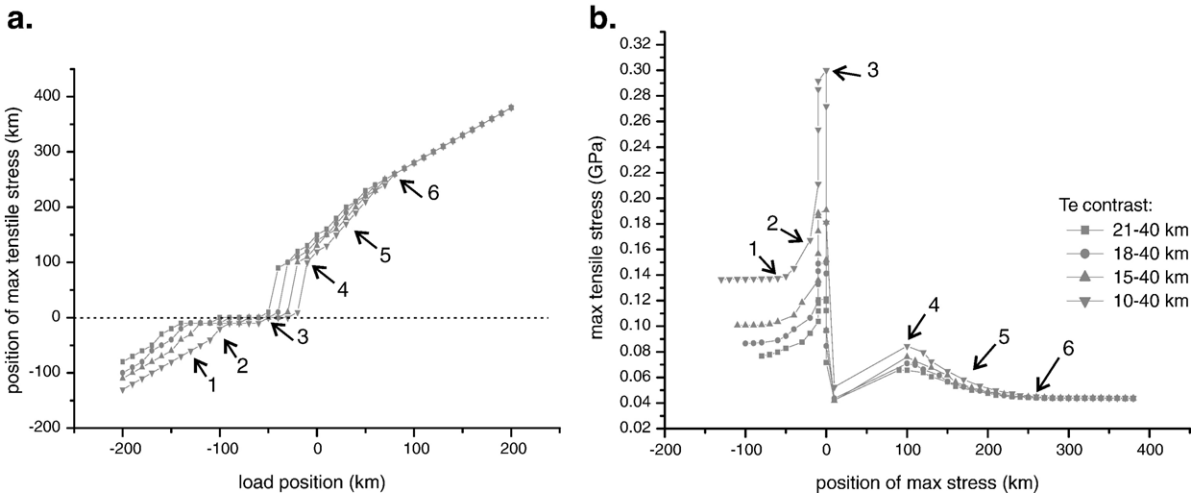

Fig. 9. (a) Position and (b) magnitude of maximum bending stress for different strength contrasts. (See also caption of Fig. 6).

minimum bulge elevation while for the 21–40 contrast the load is at −170 km. The maximum bulge elevation on the other hand occurs on a much smaller interval of load positions: the load is at $x=-20$ for the 10–40 contrast and at $x=-40$ for the 21–40 contrast. The bulge elevation maxima are different for the different contrasts. The bulge in the 10–40 contrast reaches a maximum elevation of almost twice the Te40 value (32 m), and a minimum elevation of only 0.24 times the Te40 value (4 m). For the 21–40 contrast these ratios are 1.5 and 0.56 respectively.

3.2.2. Bending stress

Stress concentration occurs at the strength transition for all Te contrasts (Fig. 9a). This lasts for a period of up to 10 load steps for the 10–40-km transition. The magnitude of the Te contrast significantly affects the magnitude of the stress increase. The 21–40 contrast results in a stress increase by a factor of 1.6 with respect to the Te21 value (from 76 to 120 MPa) before it decreases to the Te40 value (of 44 MPa); the 10–40 contrast causes a factor 2.2 increase (from 137 to 300 MPa), see Fig. 9b.

The stress increases and decreases during the period that its position is concentrated around $x=0$ (see the interval confined by arrows 2–4 in Fig. 9a and b). The initiation of the stress increase (load step 1) occurs when the load is at $x=-110$ km. Maximum stress is reached at load step $x=-50$ km (3) when its position is still at $x=0$. The eastward jump (step 4, load at $x=-10$ km) of the maximum stress position (from $x=10$ to 100 km) is accompanied by a new minor stress peak. Finally, the stress gradually decreases (5) until the characteristic Te40 stress position and value are attained (6).

3.3. Summary of model results

3.3.1. Basin geometry

In the previous sections, the changes in basin geometry and bending stress as a result of progressive loading across a transition in flexural rigidity were described in detail. The magnitudes of the changes and the load position at which they occur are dependent on the gradient of the transition. However, the general trends in the evolving basin geometry and their correlations are the same in all experiments (Fig. 10 and caption).

3.3.2. Bending stress

Our modeling showed a distinct increase of the (maximum) bending stress at the strength transition. The amplification is an effect of stress concentration around the discontinuity represented by the strength transition (Gere, 2001; pp. 139, 376). The magnitude of the increase is a function of the gradient of the transition (or the size of the discontinuity). The distance at which the stress starts increasing is a function of the strength of the plate (cf Saint-Venant's principle discussed in Gere, 2001). This is best shown in Fig. 9b when comparing the onset of stress increase for the 10–40 and 21–40 contrasts. Importantly, the maximum bending stress value is attained during the period that the site of maximum stress is fixed around the Te transition. As a result of this, the load position for which the maximum value is attained is relatively constant and the stress does not show a consistent correlation with the basin geometry (Fig. 10). Depending on the width of the transition, the number of load steps that the position of the maximum stress is fixed along the transition,

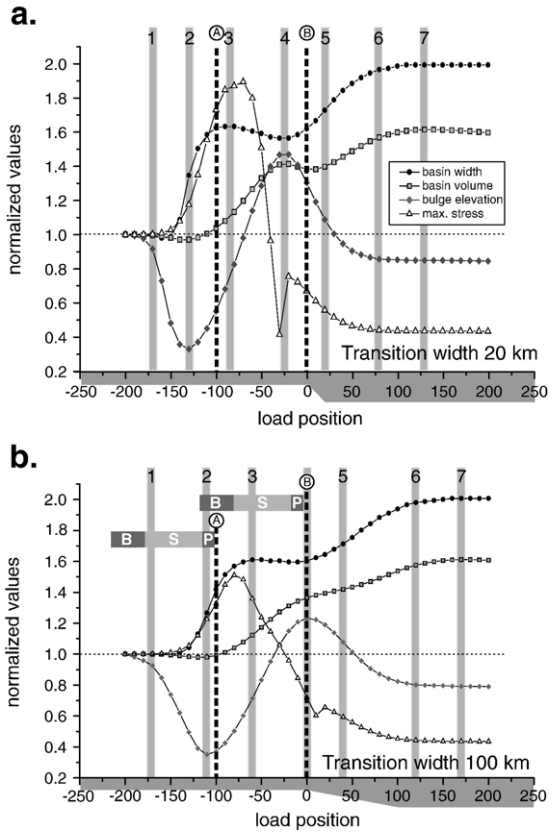

Fig. 10. Normalized model results showing the correlation between changes in basin geometry and magnitude of bending stress across the (a) 20-km and (b) 100-km wide transition from Te15 to Te40. Grey columns indicate selected load steps (cf. numbered arrows in Figs. 6–9). The first response to the strength transition is lowering of the bulge (load step 1). The lowest bulge elevation (2) corresponds to the maximum rate of basin widening and minimum basin volume. Stable basin width (3) corresponds to the maximum rate of basin volume increase. Maximum bulge elevation (4) is attained while basin width and volume are (still) stable. The initiation of a second phase of basin widening (5) is associated with a sub-minimum in basin volume and lowering of the bulge. After this load step, the basin width and volume increase and the bulge elevation is gently decreasing until the new equilibrium values are attained (6–7). The load step at which maximum bending stress is attained depends on transition width: after step 3 for the 20-km wide transition and between 2 and 3 for the 100-km wide one. Correlation with Carpathian foredeep events: Black dashed columns represent the present day situation along cross sections A and B (see Figs. 11 and 12). Horizontal bars in (b) indicate B, Badenian; S, Sarmatian; and P, Pliocene to Recent load steps along cross section A.

changes: the smaller the transition width, the larger the number of load steps (see Fig. 7c). The position of the stress is less sensitive to the strength contrast. For all contrasts (except the 10–40 contrast) the number of load steps is equal ($n=10$), and thus determined by the transition width of 20 km.

4. Application to the East Carpathian foredeep

Our modeling has shown that a strength transition can cause rapid changes in the geometry of a foredeep, even if all other parameters (rate of shortening and sedimentation; sea level; widening of the orogenic load) are constant. In the following we propose to explain the Late Miocene evolution of the East Carpathians foredeep/Focşani Depression by a model involving the strength transition from Moesian Platform to East European Craton. We will first introduce the tectonic setting and then discuss our model predictions for the area.

4.1. Romanian Carpathians and its foreland: tectonic setting

The Carpathians are a highly arcuate orogen that formed in response to the Alpine collision between the Apulian upper plate margin and related microplates, and the relatively stable foreland represented by the East-European, Scythian and Moesian blocks (Royden and Karner, 1984; Sandulescu, 1988; Csontos, 1995, and references therein). The East Carpathians are its NW–SE striking section that crosses Poland, the Ukraine and Romania. The Carpathian belt is subdivided in two domains, the Inner Carpathians (or Dacides) and the Outer Carpathian flysch belt (Moldavides).

The Inner Carpathians obtained much of their present shape and topography during Cretaceous thrusting related to the closing of the Dacidian Trough which had been formed during Late Jurassic extension. The arcuate shape of the Carpathian belt originates from this time. A second stage of contraction forming the Outer Carpathians occurred during the Neogene (Late Badenian–Sarmatian, 15–9 Ma) and involved shortening of the Moldavidian flysch basin, which had developed on (thinned) continental crust during Paleogene–Earliest Miocene time. No differential rotations are recorded during this stage. Roure et al. (1993) reconstructed from balanced cross sections a (minimum) total Neogene shortening of some 130 km in the Romanian East Carpathians, 20 km of which occurred during Pliocene or even Pleistocene time. It must be noted that the actual amount of basement shortening during the Neogene is difficult to constrain, as the Outer Carpathian flysch units are almost entirely detached from their initial pre-Cretaceous substratum (Roure et al., 1993). The end of thrusting is dated as Sarmatian by sediments sealing the frontal thrust near Trotus valley (Sandulescu, 1988). Minor shortening is recorded in the Carpathian Bend Zone as recent as Pleistocene (Walachian phase, see Hippolyte and Sandulescu (1996); Leever et al. (submitted for publication)).

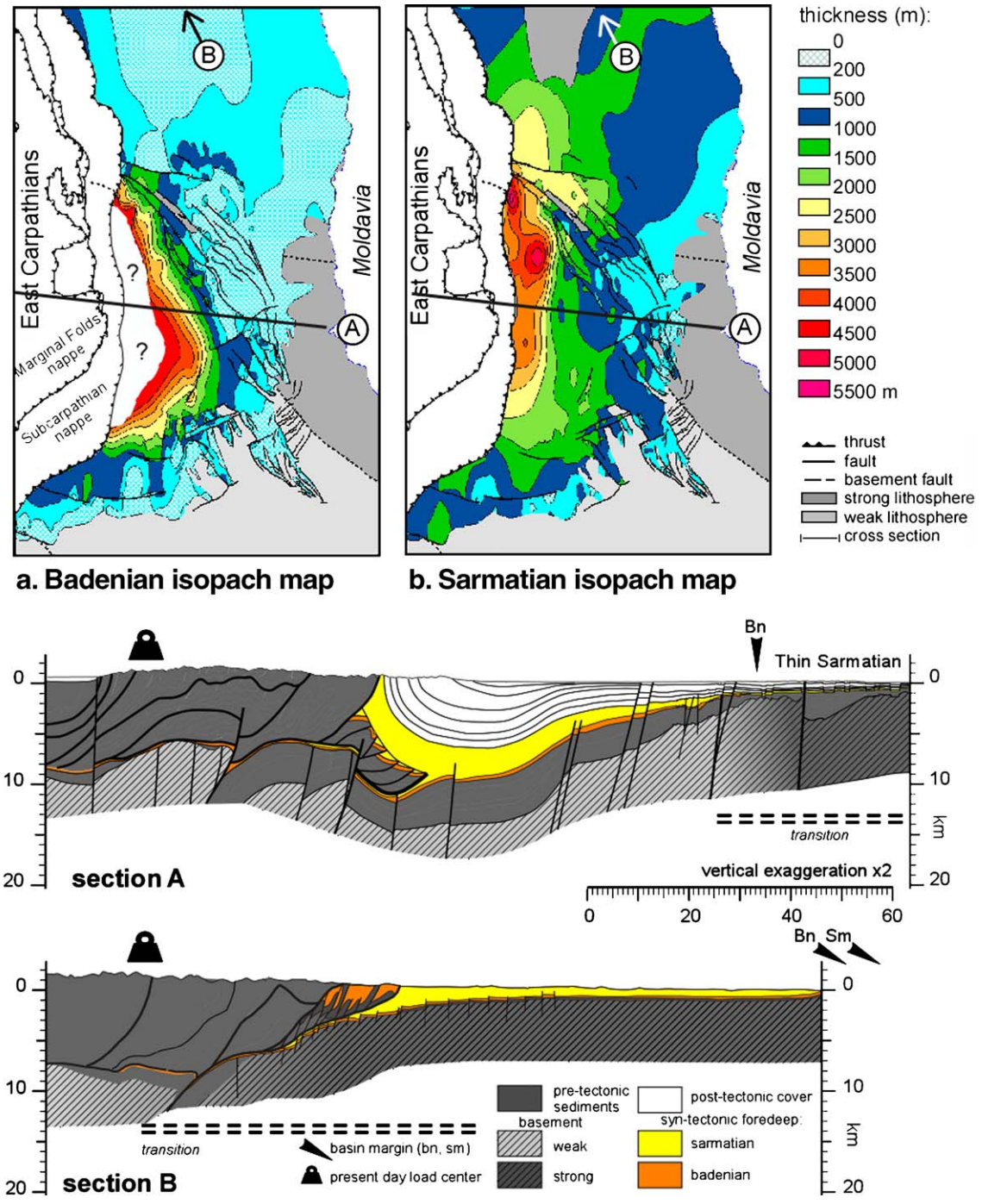

Fig. 11. (a) Badenian (16.4–12.5 Ma) and (b) Sarmatian (12.5–10.5 Ma) isopach maps of the Romanian East Carpathian Foreland–Focşani Depression. (c) cross sections. Section A (after Matenco et al., submitted for publication) crosses the Focsani Depression. Note the large thickness of post orogenic sediments, beyond the scope of this paper. Section B (after section A11 from Stefanescu et al.; Matenco and Bertotti, 2000).

The foreland of the northern part of the Romanian East Carpathians is the strong, old, cold East European Craton, part of Baltica whose lithosphere has been undisturbed since Late Proterozoic time. It is bounded in the southwest by the Tornquist–Teysseire zone, a dextral shear zone along which Baltica- and later Gondwana-derived terranes accreted during Paleozoic time (Pharaoh, 1999). These comprise (from N–S, see

also Fig. 1) the Scythian Platform, North Dobrogean Orogen and Moesian Platform.

The latter experienced a stage of rifting in the Badenian (16.5–13 Ma, Tărăpoancă et al., 2004), causing weakening of the lithosphere. The contrast in strength between the East European Craton and the terranes in the TESZ (Pharaoh, 1999) is evident from flexural modelling studies. Zoetemeijer et al. (1999) derived for the West Carpathian foreland elastic thicknesses between 16 to as little as 3 km; Royden and Karner (1984) propose a Te of 30 km in the Ukrainian East Carpathian Foreland. In contrast, Lazauskiene et al. (2002) infer a Te of >55 km (and up to 200 km) for the EEC in the Baltic region.

4.2. Effect of a lithospheric strength transition on the Late Miocene evolution of the East Carpathian foredeep

The East Carpathian foredeep formed as a result of Neogene shortening. Its syntectonic evolution will be discussed in more detail below. The part of the foredeep situated on top of the Moesian Platform, known as the Focşani Depression, is furthermore characterized by anomalously large subsidence which postdates the Late Miocene 'normal' foredeep stage and cannot be related to only topographic loading (Fig. 11c, Royden and Karner, 1984; Tărăpoancă et al., 2004; Cloetingh et al., 2004, Matenco et al., submitted for publication; Leever et al., submitted for publication). The post-Sarmatian evolution of the basin is beyond the scope of this paper.

4.2.1. East Carpathian foredeep geometry

Fig. 11 (adapted from Tărăpoancă et al., 2003) shows the sediment thicknesses of the East Carpathian foreland in two Late Miocene stages (Badenian and Sarmatian). These are seen to display very distinct patterns. In the Focşani Depression, accommodation space for the Early Badenian sediments was generated by rifting (Tărăpoancă et al., 2004). Late Badenian sediments were deposited in the early foredeep stage, at the onset of renewed shortening in the Carpathians (Moldavidian phase), and during this period the orogenic front was at a distance of approximately 120–90 km from its present position. Continental collision and blocking of the system occurred in the Sarmatian (13–10 Ma), during which time the belt was displaced an additional 70 km to its final position (Roure et al., 1993). The Badenian basin is mainly constrained to the Moesian Platform, bounded to the east by the Peceneaga–Camena Fault (PCF). Where Badenian sediments do occur on the EEC, their thickness is generally less than 500 m and over large areas no more than 200 m. In contrast, Sarmatian sediments do reach considerable thicknesses, >2000 m, in the same area. The Sarmatian basin is widest in the north, where it overlies the EEC. For basin width see also Fig. 13a, adapted from Saulea et al. (1969). An almost regional unconformity forms the boundary between Badenian and Sarmatian sediments in the southern part of the study area (Focsani Basin).

4.2.2. Model parameters

Fig. 12 shows a schematic tectonic map of the Romanian East Carpathians. The elements relevant to our modelling are the orogenic belt and the foreland, of which the latter is composed of the strong East European Craton (EEC) and the Moesian Platform, separated by the Tornquist–Teisseyre Zone (TTZ). In the north, the N–S striking orogenic belt has overthrust the northern continuation of the Moesian Platform and lies on top of the EEC, while in the south, the thrust front is still at a large distance to the transition and lies on top of the Moesian Platform. From previous flexural modelling (Tărăpoancă et al., 2004) we adopted the Te values of 15

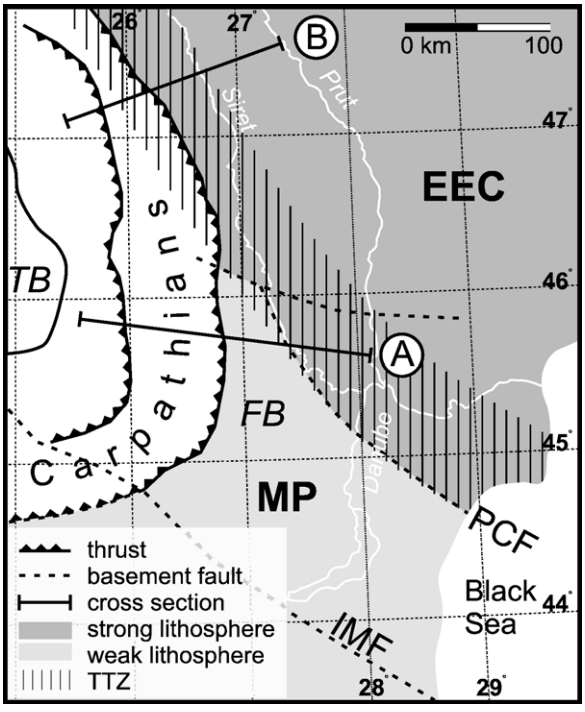

Fig. 12. Schematic tectonic map of the Romanian East Carpathians and its foreland, showing the obliquity between the orogen and the strength transition. Cross sections A and B represent different load steps (see Figs. 10 and 11). EEC=East European Craton, MP=Moesian Platform; FB=Focşani Basin, TB=Transylvanian Basin; IMF=Intra-Moesian Fault, PCF=Peceneaga–Camena Fault; hatched area=Tornquist Teisseyre Zone.

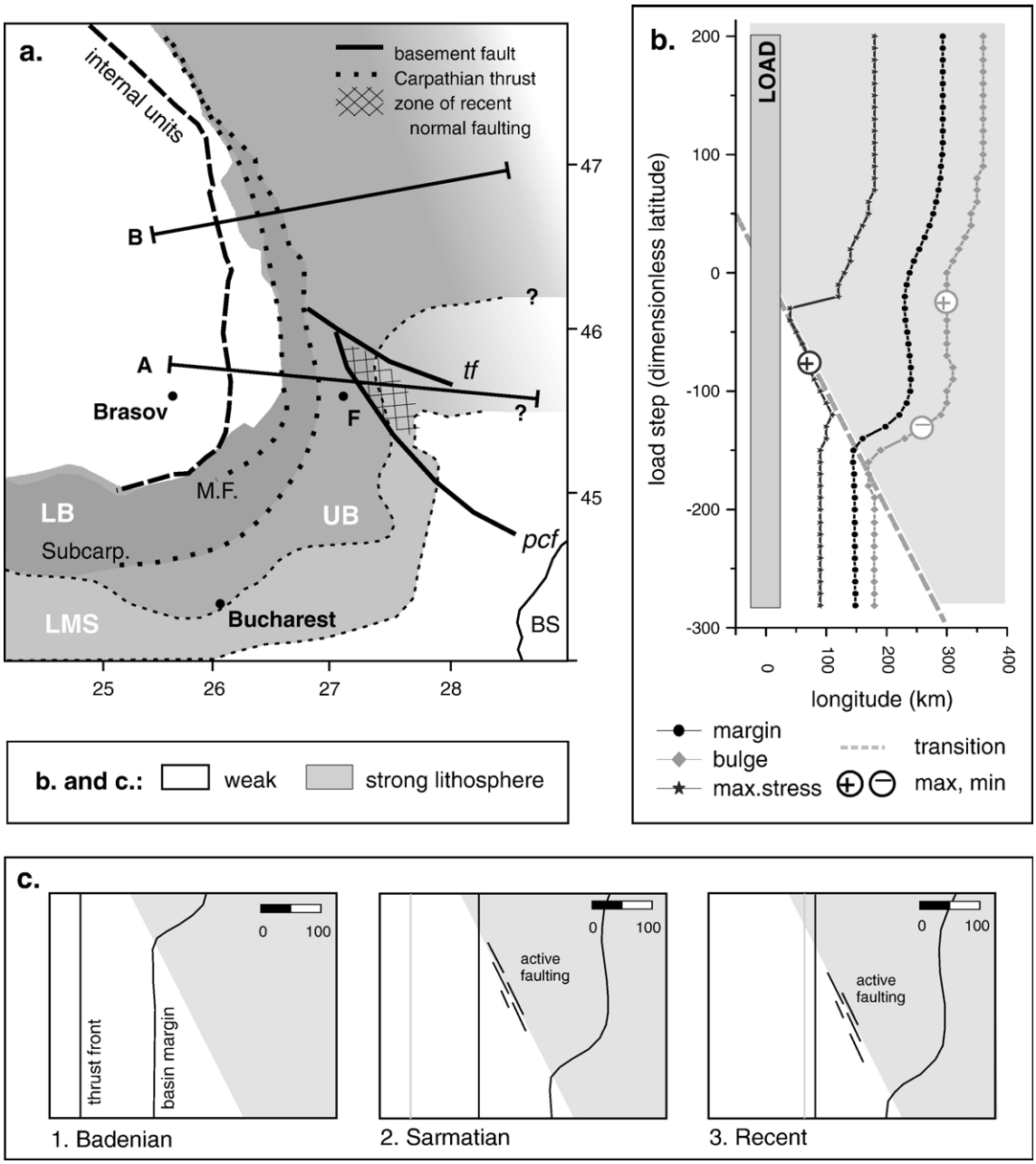

Fig. 13. (a) Map (after Saulea et al., 1969) showing occurrence of Lower Badenian (LB), Upper Badenian (UB), Lower–Middle Sarmatian (LMS) sediments and location of active normal faulting. M.F., Marginal Folds Nappe; PCF, Peceneaga–Camena Fault; TF, Trotus Fault; F, Focsani; BS, Black Sea. (b) Model results for the 100-km wide strength transition (Te 15–40 km) where load position is plotted as dimensionless latitude. (c) Evolutionary model for East Carpathian foredeep.

and 40 km in our model for the Moesian Platform (west) and EEC (east) respectively. The width of the TTZ (i.e. the transition zone) is some 80–100 km, with its western termination to Moesia situated at the Peceneaga–Camena Fault (PCF). The same load and basin fill as in the previous runs was assumed (Table 1).

We will present and discuss our model results along two cross sections (Fig. 11c, location in Fig. 12). For section *A*, the present distance between the load and the transition zone (PCF) is ca. 100 km. At section *B*, the transition is covered by the belt. We assume the present distance between the transition and the load center to be 0 km.

4.2.3. Model results

Bearing in mind the limitations of the 2D model, the obliquity between the orogenic belt and the strength transition allows making a virtual step from time to space: the geometry along a cross section in the south (*A*) would correspond to an earlier load step than the one in the north (*B*) (see Figs. 11c, 12, 13a). The present day load positions along cross sections *A* and *B* are indicated in Fig. 10, both for the reference model discussed below (100-km wide transition, Fig. 10b) and the 20-km wide transition (Fig. 10a). Assuming maximum basement consumption, the Early Badenian load position at cross section *A* is restored to a distance of approximately 220 km from the transition to the EEC. At this time, or load step, the basin geometry is at equilibrium for the Moesian Platform strength (Te = 15 km, Fig. 13a). During Badenian, the load migrated some 50 km towards the east. During this period, our model predicts constant basin width, volume and bending stress, and onset of lowering of the bulge. Another 70 km of convergence occurred during Sarmatian. The bulge elevation decreases to its minimum and the basin width increases, as well as the bending stress. The basin volume is relatively unaffected. Some 20 km of Pliocene–Recent displacement results in further basin widening and stress increase, while the bulge elevation starts increasing.

Along cross section *B*, the Early Badenian load position restores to a distance of 120 km from the strength transition. Major basin widening occurs during this period while the bulge elevation is lowest and bending stresses start reaching their maximum value. In Sarmatian the maximum basin width is attained, while bending stresses decrease and basin volume starts increasing. The bulge elevation is restored to its original elevation and continues rising.

5. Discussion

5.1. Model assumptions

Increase of the size (magnitude and width) of the load, which would normally be expected in a growing orogen, was not taken into account in our models. Increasing its magnitude would affect the amplitude of the signal but not its wavelength nor the correlation. However, the changing width of the orogen does affect the basin width as is shown by DeCelles and DeCelles (2001), who propose a model to derive rates of orogenic shortening from observed rates of flexural bulge migration. They assume the rate of bulge migration to be the sum of the rate of convergence (load migration) and widening of the orogen by accretion (thrust front migration).Typically, for parameters compatible with the Carpathians, the rate of bulge migration resulting from widening of the orogen is some 1.5 times the convergence rate, comparable to our results for the 200-km wide transition (Fig. 6a). Widening of the orogen should thus be taken into account when studying the evolution of foredeep geometry. Conversely, the significant basin widening across a strength transition (at rates of >4 times the convergence rate following our results) would cause their model to seriously overestimate the actual shortening rates.

We assumed the position of the basin margin to be at $w(x)=0$; however, eustasy and overfilling of the basin may cause adaptation of actual deposition limit, as shown by Flemings and Jordan (1989) who found that efficient sediment transport will cause a wide basin when all other parameters are constant.

5.2. Application to East Carpathian foredeep

The model (Fig. 10b) predicts along cross section *B* a rapid increase of basin width, from the initially small value associated with the weak western plate to the large width associated with the strong EEC. This result is in agreement with the data that show a rapid invasion of the foreland by Sarmatian sediments (Figs. 11, 13a, and see also seismic sections in Tărăpoancă et al., 2003). For the strength contrast and transition width we assumed, the model predicts significant basin widening in Sarmatian time also at the location of section *A*. Moreover, the location of presently active normal faulting (Figs. 11, 13a) is correctly predicted by the model, for even with an additional 20 km of Pliocene–Recent displacement, the maximum bending stresses would still be situated along the strength transition (or PCF).

Part of the observed basin widening may be due to widening of the orogenic load. During the ~ 6 Ma of Badenian–Sarmatian convergence, the flysch belt attained a width of ~ 50 km (55 km along section A, 40 along section B), implying a propagation rate of the front of the belt of ~ 8 mm/y additional to the shortening rate of ~ 20 mm/y (conventions as in DeCelles and DeCelles, 2001). The predicted basin margin/bulge migration rate is therefore on average 1.4 times the load migration rate due to widening effects only, and would imply a 170 km eastward displacement of the basin margin while the load itself moves 120 km, resulting in 50 km basin widening along the entire length of the belt. For a (constant) plate strength of Te = 15 km, the basin width would increase by a factor of 1.3 from 150 to 200 km. According to our model results, the strength transition causes, along section *B*, a widening of ~ 90 km during Badenian and earliest Sarmatian convergence. Basin width is subsequently

constant, the migration of the margin occurring at the load migration/shortening rate. The increase in migration rate due to the strength transition is much larger than the one caused by widening of the load but occurs over a shorter time interval. Moreover, the distinct difference in distribution of Sarmatian sediments over the EEC and Moesian Platform (Fig. 13a) can only be explained by the strength transition.

An evolutionary model is proposed in Fig. 13c (compare with Fig. 13a), showing the progressive change of the basin shape and position with time. In the Badenian, the foredeep is constrained to the Moesian Platform and its width determined by the rigidity of that plate. The regional erosional unconformity at the Badenian–Sarmatian boundary (Tărăpoancă et al., 2004) can be explained by the passing of the flexural bulge across the present day Focsani depression. During Sarmatian convergence the widened basin starts invading the foreland further south. Large bending stresses and associated normal faulting are predicted along the PCF. The Badenian basin is largely overthrust by the advancing belt.

The large overall subsidence (Royden and Karner, 1984) and particularly the major post-orogenic subsidence in the area (Fig. 11c, Tărăpoancă et al., 2003), is supposedly associated with a remnant slab. A number of geodynamical models have been proposed, mostly conceptual (Artyushkov et al., 1996; Mason et al., 1998; Nemcok et al., 1998, Chalot-Prat and Girbacea, 2000; Sperner et al., 2004; Cloetingh et al., 2004). This points to anomalous conditions in the Carpathian Bend Zone, yet our simple flexural model assuming only topographic loading gives a reasonable first order explanation of the observed changes in basin shape and position, and active faulting.

6. Conclusions

We showed that a strength transition in the foreland of an advancing orogen will influence the shape and bending stresses in the pro-foredeep. With all other basin forming parameters constant, a transition from weak to strong lithosphere will cause an increase the rate of migration of the distal basin margin (i.e. the basin width), result in oscillation of the flexural bulge, and will tend to confine and amplify the bending stresses around the transition.

We did not aim to reproduce in detail the geometry of the East Carpathian foredeep, rather, to explore the influence of different lithospheric domains in the foreland on foredeep evolution. The model predictions give a reasonable first order explanation of the Late Miocene evolution of the Romanian East Carpathian foredeep.

In Badenian time, the load was still far removed from the transition to the strong lithosphere of the EEC. The basin was constrained to the Moesian platform and its width determined by the rigidity of this plate; the flexural bulge being located at the present day Focsani Depression. At some point in Sarmatian time, the load has approached the strength transition to such a distance that the basin starts invading the EEC progressively southwards. Normal faulting persisting along the strength transition is predicted as an effect of enhanced bending stresses.

References

Artyushkov, E.V., Baer, M.A., Mörner, N.-A., 1996. The East Carpathians: indications of phase transitions, lithospheric failure and decoupled evolution of thrust belt and its foreland. Tectonophysics 262, 101–132.

Bertotti, G., Ter Voorde, M., Cloetingh, S.A.P.L., Picotti, V., 1997. Thermomechanical evolution of the South-Alpine rifted margin (north Italy): constraints on the strength of passive continental margins. Earth and Planetary Science Letters 146, 181–193.

Bodine, J.H., Watts, A.B., 1979. On lithospheric flexure seaward of the Bonin and Mariana trenches. Earth and Planetary Science Letters 43, 132–148.

Bodine, J.H., Steckler, M.S., Watts, A.B., 1981. Observations of flexure and the rheology of the oceanic lithosphere. Journal of Geophysical Research 86 (B5), 3695–3707.

Burov, E., Diament, M., 1995. The effective elastic thickness of continental lithosphere: what does it really mean? Journal of Geophysical Research 100 (B3), 3905–3927.

Chalot-Prat, F., Girbacea, R., 2000. Partial delamination of continental mantle lithosphere, uplift-related crust–mantle decoupling, volcanism and basin formation: a new model for the Pliocene–Quaternary evolution of the southern East-Carpathians, Romania. Tectonophysics 327, 83–107.

Clevis, Q., De Boer, P.L., Nijman, W., 2004. Differentiating the effect of episodic tectonism and eustatic sea-level fluctuations in foreland basins filled by alluvial fans and axial deltaic systems: insights from a three-dimensional stratigraphic forward model. Sedimentology 51 (4), 809–836.

Cloetingh, S.A.P.L., Burov, E., Matenco, L., Toussaint, G., Betrotti, G., Andriessen, P.A.M., Wortel, M.J.R., Spakman, W., 2004. Thermo-mechanical controls on the mode of continental collision in the SE Carpathians (Romania). Earth and Planetary Science Letters 218 (1), 57–76.

Csontos, L., 1995. Tertiary tectonic evolution of the Intra-Carpathian area: a review. Acta Vulcanologica 7, 1–13.

Davison, I., 1997. Wide and narrow margins of the Brazilian South Atlantic. J. Geol. Soc. (London) 154, 471–476.

DeCelles, P.G., DeCelles, P.C., 2001. Rates of shortening, propagation, underthrusting, and flexural wave migration in continental orogenic systems. Geology 29 (2), 135–138.

DeCelles, P.G., Giles, K.A., 1996. Foreland basin systems. Basin Research 8, 105–123.

Desegaulx, P., Kooi, H., Cloetingh, S.A.P.L., 1991. Consequences of foreland basin development on thinned continental lithosphere: application to the Aquitaine basin (SW France). Earth and Planetary Science Letters 106, 116–132.

Flemings, P.B., Jordan, T.E., 1989. A synthetic stratigraphic model of foreland basin development. Journal of Geophysical Research 94 (B4), 3851–3866.

Garcia-Castellanos, D., 2002. Interplay between lithospheric flexure and river transport in foreland basins. Basin Research 14, 89–104.

Gere, J.M., 2001. Mechanics of Materials. Nelson Thornes, Cheltenham.

Hippolyte, J.-C., Sandulescu, M., 1996. Paleostress characterization of the "Wallachian phase" in its type area (southeastern Carpathians, Romania). Tectonophysics 263, 235–248.

Johnson, D.D., Beaumont, C., 1995. Preliminary results from a planform kinematic model of orogen evolution, surface processes and the development of clastic foreland basin stratigraphy, stratigraphic evolution of foreland basins. Spec. Publ. Soc. Econ. Paleontol. Mineral. Society for sedimentary geology, Tulsa, Oklahoma, pp. 3–24.

Lazauskiene, J., Stephenson, R.A., Sliaupa, S., Van Wees, J.D., 2002. 3-D flexural modelling of the Silurian Baltic Basin. Tectonophysics 346, 115–135.

Leever, K., Matenco, L., Bertotti, G., Cloetingh, S. Drijkoningen, K.G., submitted fo publication. Late orogenic vertical movements in the Carpathian Bend Zone from seismic constraints on the transition zone from orogen to foredeep. Basin Research.

Mason, P.R.D., Seghedi, I., Szákacs, A., Downes, H., 1998. Magmatic constraints on geodynamic models of subduction in the East Carpathians, Romania. Tectonophysics 297, 157–176.

Matenco, L., Bertotti, G., 2000. Tertiary tectonic evolution of the external East Carpathians (Romania). Tectonophysics 316, 255–286.

Matenco, L., Bertotti, G., Leever, K, Cloetingh, S., Schmid, S., Tarapoanca, M., Dinu, C., submitted for publication. Large scale deformations during the post-orogenic evolution of locked collisional boundary: coeval Pliocene–Quaternary differential tectonic movements of the SE Carpathians foreland.

Matenco, L., Zoetemeijer, R., Cloetingh, S.A.P.L., Dinu, C., 1997. Lateral variations in mechanical properties of the Romanian external Carpathians: inferences of flexure and gravity modelling. Tectonophysics 282, 147–166.

Nemcok, M., Pospisil, L., Lexa, J., Donelick, R.A., 1998. Tertiary subduction and slab break-off model of the Carpathian–Pannonian region. Tectonophysics 295, 307–314.

Pérez-Gussinyé, M., Watts, A.B., 2005. The long-term strength of Europe and its implications for plate-forming processes. Nature 436, 381–384.

Pharaoh, T.C., 1999. Palaeozoic terranes and their lithospheric boundaries within the Trans-European Suture Zone (TESZ): a review. Tectonophysics 314, 17–41.

Ranalli, G., 1995. Rheology of the Earth. Chapman & Hall, London.

Roure, F., Roca, E., Sassi, W., 1993. The Neogene evolution of the outer Carpathian flysch units (Poland, Ukraine and Romania): kinematics of a foreland/fold-and-thrust belt system. Sedimentary Geology 86, 177–201.

Royden, L.H., Karner, G.D., 1984. Flexure of lithosphere beneath Apennine and Carpathian foredeep basins: evidence for an insufficient topographic load. AAPG Bulletin 68 (6), 704–712.

Sandulescu, M., 1988. Cenozoic tectonic history of the Carpathians. In: Royden, L.H., Horvath, F. (Eds.), AAPG Memoir, pp. 17–25.

Saulea, E., Popescu, I., Săndulescu, J., 1969. Lithofacies Atlas. Institutul de Geologie şi Geofizică.

Sperner, B., Ioane, D., Lillie, R.J., 2004. Slab behaviour and its surface expression: new insights from gravity modelling in the SE-Carpathians. Tectonophysics 382, 51–84.

Stewart, J., Watts, A.B., 1997. Gravity anomalies and spatial variations of flexural rigidity at mountain ranges. J. Geophys. Res. 102 (B3), 5327–5351.

Stockmal, G.S., Beaumont, C., Boutilier, R., 1986. Geodynamic models of convergent margin tectonics: transition from rifted margin to overthrust belt and consequences for foreland basin development. AAPG Bulletin 70, 181–190.

Tărăpoancă, M., 2004. Architecture, 3D geometry and tectonic evolution of the Carpathians Foreland Basin. PhD Thesis, Vrije Universiteit, Amsterdam, 119 pp.

Tărăpoancă, M., Bertotti, G., Matenco, L., Dinu, C., Cloetingh, S.A.P.L., 2003. Architecture of the Focşani depression: a 13 km deep basin in the Carpathians bend zone (Romania). Tectonics 22 (6).

Tărăpoancă, M., Garcia-Castellanos, D., Bertotti, G., Matenco, L., Cloetingh, S.A.P.L., Dinu, C., 2004. Role of the 3-D distributions of load and lithospheric strength in orogenic arcs: polystage subsidence in the Carpathians foredeep. Earth and Planetary Science Letters 221 (1–4), 163–180 (30 April).

Turcotte, D.L., Schubert, G., 2002. Geodynamics. Cambridge University Press, Cambridge.

Van Wijk, J.W., 2002. Passive margin formation: tectonic modelling of pre- and synrift lithospheric controls. PhD Thesis Vrije Universiteit, Amsterdam.

Waschbusch, P.J., Royden, L.H., 1992. Episodicity in foredeep basins. Geology 20, 915–918.

Watts, A.B., Bodine, J.H., Steckler, M.S., 1980. Observations of flexure and the state of stress in the oceanic lithosphere. J. Geophys. Res. 85 (B11), 6369–6376.

Willett, S., Beaumont, C., Fullsack, P., 1993. Mechanical model for the tectonics of doubly vergent compressional orogens. Geology 21 (4), 371–374.

Wu, P., 1991. Flexure of lithosphere beneath the Alberta foreland basin: evidence of an eastward stiffening continental lithosphere. Geophysical Research Letters 18 (3), 451–454.

Zoetemeijer, R., 2000. Lithosphere under the outer Carpathian Arc; breaking (and shaking?) at the contacts between strong and weak. Geophysical Research Abstracts 2.

Zoetemeijer, R., Tomek, C., Cloetingh, S.A.P.L., 1999. Flexural expression of European continental lithosphere under the western outer Carpathians. Tectonics 18 (5), 843–861.